INTECH
open science | open minds

OPEN ACCESS
ARTICLE

International Journal of Advanced Robotic Systems

# Kinematics and Dynamics of a New 16 DOF Humanoid Biped Robot with Active Toe Joint

Regular Paper

C. Hernández-Santos[1], E. Rodriguez-Leal[1,*], R. Soto[1] and J.L. Gordillo[1]

1 Center for Robotics and Intelligent Systems, Tecnológico de Monterrey, Campus Monterrey, México
* Corresponding author E-mail: ernesto.rodriguez@itesm.mx

Received 16 May 2012; Accepted 17 Aug 2012

DOI: 10.5772/52452

© 2012 Hernández-Santos et al.; licensee InTech. This is an open access article distributed under the terms of the Creative Commons Attribution License (http://creativecommons.org/licenses/by/3.0), which permits unrestricted use, distribution, and reproduction in any medium, provided the original work is properly cited.

Abstract Humanoid biped robots are typically complex in design, having numerous Degrees-of-Freedom (DOF) due to the ambitious goal of mimicking the human gait. The paper proposes a new architecture for a biped robot with seven DOF per each leg and one DOF corresponding to the toe joint. Furthermore, this work presents close equations for the forward and inverse kinematics by dividing the walking gait into the Sagittal and Frontal planes. This paper explains the mathematical model of the dynamics equations for the legs into the Sagittal and Frontal planes by further applying the principle of Lagrangian dynamics. Finally, a control approach using a PD control law with gravity compensation was recurred in order to control the desired trajectories and finding the required torque by the joints. The paper contains several simulations and numerical examples to prove the analytical results, using SimMechanics of MATLAB toolbox and SolidWorks to verify the analytical results.

Keywords Humanoid Robot, Degrees-of-Freedom, Lagrangian Dynamics, Control

## 1. Introduction

In recent years, several efforts of the robotics community have focused on developing bio-inspired robots, particularly in humanoid biped robots. This has resulted in promising developments such as the ASIMO (the acronym of "Advanced Step In Mobility") humanoid robot, developed by Honda with 32 DOF and 52 kg weight [1] or the 62-kg MAHRU series of Samsung Electronics with 32 DOF [2]. Further examples of contributions in the humanoid robots field are the QRIO, which has an adaptable motion controller that allows the displacement on uneven surfaces and external forces [3] and the WABIAN series of Waseda University with 35 DOF [4], which has played a fundamental role in the evolution of humanoid robots. Some of the most studied architectures found in the literature include the H7 from the University of Tokyo with a total of 30 DOF, seven for each leg including a one DOF toe joint, seven DOF for each arm, including a single DOF gripper and two DOF at the neck [5]. Another example is the JOHNNIE robot from the Technical University of Munich, where each leg incorporates six driven joints, three DOF in the hip, one

DOF for the knee, and another two DOF for the ankle joint [6]. Nowadays, most of the humanoid robots mentioned above consist of two 6-DOF legs, namely 3-DOF hip, 1-DOF knee and 2-DOF ankle. Although the efforts have mainly focused on achieving human gait, this feature has not been successful accomplished with a limited number of DOF. Thus, it becomes necessary to incorporate redundant DOF in order to achieve an approximate human gait motion [7].

The addition of an active toe joint to the kinematic model of each leg has drawn enormous interest within the robotics scholars, because compared with conventional humanoid robots that are equipped with flat feet, this architecture allows a robot to walk in a more natural way. There are several references in the literature related to toe joints in biped robots. For example, Kumagai et al. developed a biped robot which has 7 DOF at each leg including a passive toe joint [8]. Kumazawa et al. [9] and Ogura et al. [10] proposed an elastic toe joint mechanism; the passive joint, which was selected by analysing human gait analysis reports. The toe joint was then developed as a hinge joint. However, in order to improve the toe functionality, an active joint control is required for keeping a multipoint contact with the floor. Konno et al. [11] included passive toe joints with torsion springs in order to achieve human-like gait based on biomechanical studies. Scarfogliero et al. [12] equipped the passive toe joints with spring-damper buffers for a smoother foot rotation. Koganezawa et al. [13] proposed a hybrid active/passive design for lower energy consumption during walking. Nishiwaki et al. [14] added an active toe joint to each 6 DOF leg to achieve high walking speed, high step climbing, and knee down motion with the sole attached to the ground. Furthermore, the authors used toe joint rotation during the double support phase to decrease the knee joint angular velocity, resulting in a 1.8 times faster gait motion due to the active toe joints. Nevertheless, using the toe joint only in the double support phase, strongly limits the advantages introduced by this feature. In fact, during the double support phase it is also possible to introduce a foot rotation about the front edge, which leads to similar results. Finally, the gait results in an unnatural motion due to the fact that the humanoid cannot stretch the knees. Sellaouti et al. [15] focused on walking speed augmentation in a 6 DOF leg through the use of passive toe joints during the single support phase, achieving a 1.5 times faster gait motion. This result is due to the integration of an under actuated phase at the end of the single support phase, where the support foot rotates around the toe joint and allows the ankle joint to rise. It was also noticed that when passing the straight leg singularity, the robot was able to fulfil larger steps and increase its walking speed. This robot however, has an unnatural gait, since the humanoid has to lower its centre of mass closer to the ground in order to get large steps. Kumar et al. [16] presented a 2 DOF leg with a passive toed feet that can walk down a gentle slope under the action of gravity alone using ankle-strike as a mean to progress to toe-rotation phase. The lack of an active joint prevents this architecture to walk on any other surface than a downward slope. From the abovementioned robotic architectures, the development of a robotic leg with more than 6 DOF and an active toe joint that would enable walking in a more natural manner has yet to be proposed.

This paper suggests a new architecture for a biped robot with seven DOF per leg, adding one DOF that imitates the toe joint. In this kinematic chain all the joints are active, in contrast to the previously mentioned architectures, which have six or seven DOF without a toe joint or with a passive toe joint. The authors believe that with this new architecture, the humanoid robot will be able to walk with the knee stretched. This is due to the fact that the walking patterns of many biped robots are calculated by solving six dimensional inverse kinematics based on the position and orientation of the foot and the waist, meaning that the seven DOF leg would provide the necessary redundancy to avoid the singularity problem presented in humanoids. This paper presents a comprehensive study of the forward and inverse kinematics of the new architecture for a humanoid leg.

The modelling of biped gait has usually resulted in the description of kinematics, dynamics and stability of two-legged walking robots and represents an unresolved challenge, as most approaches reduce the dynamic model of the humanoid robot to an inverted pendulum that is based upon either a simple observation or mathematical analysis, derived from kinematics [17]. A different approach suggests that walking motion, with static balance, could be achieved by solving simple kinematics equations. However, the static approach results in undesirable constraints on both the biped structure and walking efficiency [18]. Although these methods are valid for studying the walking stability of a humanoid robot, they do not solve complex stability problems such as modelling the human gait motion [19]. An alternative way to derive mathematical dynamics and achieve a stable biped locomotion is the use of Lagrangian dynamics. This technique has been especially successful in providing an understanding of the unstable dynamics associated with biped posture and enables the design of effective stabilization controls for robots [20]. The Lagrange-Euler formulation has been used in [21] to solve the problem of dynamically balanced gait generation by determining the joint torques for a 7 DOF two-legged robot. The Lagrangian equation has been used in [22] to obtain the dynamic model for of a five link biped where each leg has 2 DOF, applying a conventional Proportional- Derivative (PD) controller in which the

locomotion is constrained within the Sagittal plane to control the stability of a human gait. Further studies approach the dynamics by restricting the motion for the Sagittal plane for a five link biped robot [23] and a nine-link biped robot model with 3 DOF in each leg [24]. This paper uses the Lagrangian dynamic model for finding the close-form equations that model dynamic behaviour by means of dividing the legs into the Sagittal and Frontal planes, which simplify the mathematical model and further applies PD control law with gravity compensation to determine the desired position and torque for each joint.

This paper is organized as follows. In Section 2, the forward kinematics for the proposed humanoid robot is obtained using the Denavit-Hartenberg convention. This is followed by Section 3, which presents the inverse kinematics in the Sagittal and Frontal planes. Section 4 includes trajectory planning for controlling the biped robot through periodic motion in order to produce a stable gait. The discussion about the dynamic model in the Sagittal and Frontal planes using Lagrange equations is in Section 5. Several simulation results using MATLAB SimMechanic are compared with numerical examples, which demonstrate the plausibility of the analytical equations in Section 6. Finally, Section 7 presents some important conclusions and suggestions for future research on this new architecture for a humanoid biped robot.

## 2. Forward Kinematics

In robotics literature, forward kinematics is commonly known as the task in which the position and orientation of the end-effector is to be determined by giving the configurations for the active joints of the robot [23]. This paper focuses on the lower body of a humanoid biped robot as shown in Figure 1. It consists of two 8 DOF legs, namely a 3 DOF hip, a 1 DOF knee, a 3 DOF ankle and 1 DOF that imitates the toe joint. Each leg can be modelled as a kinematic chain with nine links connected by eight revolute joints.

| Joint | | Standard human leg (deg.) | Humanoid robot (deg.) |
|---|---|---|---|
| **Waist** | Pitch | -15 to 130 | -15 to 100 |
| | Roll | -30 to 45 | 0 to 45 |
| | Yaw | -45 to 50 | -45 to 45 |
| **Knee** | Pitch | -10 to 155 | 0 to 120 |
| **Ankle** | Pitch | -20 to 50 | -30 to 40 |
| | Roll | -30 to 60 | -30 to 30 |
| | Yaw | -30 to 30 | -20 to 40 |
| **Toe** | Pitch | -60 to 60 | 0 to 60 |

**Table 1.** Joint range of motion

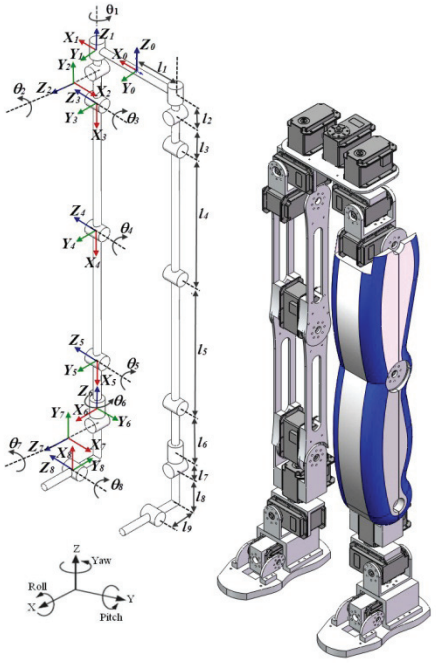


**Figure 1.** Kinematic description of the robot leg

The synthesis of the kinematic chains is based on human body parameters in terms of ratios, range of motion, and physical length [24]. Table 1 shows the range of motion for the human leg, while the parameters corresponding to the robot leg are based on a previous study by Hernandez-Santos et al [25]. Note that some ranges of motion of the humanoid robot do not correspond to the human leg, due to the interference between mechanical parts.

The local frames $(X_i, Y_i, Z_i)$ are assigned to each joint according to the Denavit-Hartenberg (DH) convention [26]. Consider the base frame $(X_0, Y_0, Z_0)$ at the centre of the waist as the global reference frame. Since the general kinematic structures of the left leg of a humanoid robot are identical to those of the right leg, this paper assigns the same coordinate frames for the left and right limbs for convenience of analysis. Figure 1 shows the designated local coordinate frames for the right leg, where $l_i$ denotes the length of link $i$. Table 2 shows the DH parameters where $\theta_i$ is the angle between the $X_{i-1}$ and $X_i$ axes as measured about the $Z_{i-1}$ axis; $d_i$ is the distance from the $X_{i-1}$ to the $X_i$ axis as measured along the $Z_i$ axis; $a_i$ is the distance from the $Z_{i-1}$ to $Z_i$ axis measured along the $X_{i-1}$ axis; and $\alpha_i$ is the angle between the $Z_{i-1}$ and $Z_i$ axes measured about the $X_{i-1}$ axis. The angles are assumed positive, counterclockwise about the rotation axis.

The position and orientation of the end-effector of a limb can be obtained by pre-multiplying the link transformation matrices together to obtain the spatial displacement of the 8*th* coordinate frame with respect to the base reference coordinate frame, namely

$$
{}^{0}T_{8} = \prod_{1}^{8} {}^{i-1}A_{i} = {}^{0}A_{1}\,{}^{1}A_{2}\,{}^{2}A_{3}\,{}^{3}A_{4}\,{}^{4}A_{5}\,{}^{5}A_{6}\,{}^{6}A_{7}\,{}^{7}A_{8}
= \begin{bmatrix} \boldsymbol{n} & \boldsymbol{s} & \boldsymbol{a} & \boldsymbol{p} \\ 0 & 0 & 0 & 1 \end{bmatrix} \tag{1}
$$

Where ${}^{i-1}A_{i}$ is a general link transformation matrix relating the *i-th* coordinate frame to the *(i-1)th* coordinate frame, $\boldsymbol{n}$ represents the normal vector, $\boldsymbol{s}$ is the sliding vector, $\boldsymbol{a}$ denotes the approach vector, and $\boldsymbol{p}$ describes the position vector of the foot [26]. According to the DH coordinate system, the homogeneous transformation of the links gives

$$
A_{i} = \begin{bmatrix} c\theta_{i} & -s\theta_{i}\cdot c\alpha_{i} & s\theta_{i}\cdot s\alpha_{i} & a_{i}\cdot c\theta_{i} \\ s\theta_{i} & c\theta_{i}\cdot c\alpha_{i} & -c\theta_{i}\cdot s\alpha_{i} & a_{i}\cdot s\theta_{i} \\ 0 & s\alpha_{i} & c\alpha_{i} & d_{i} \\ 0 & 0 & 0 & 1 \end{bmatrix} \tag{2}
$$

Where $s\theta_i = sin\ \theta_i$, $c\theta_i = cos\ \theta_i$, $s\alpha_i = sin\ \alpha_i$, and $c\alpha_i = cos\ \alpha_i$. Furthermore, by using Eq. (1) and (2), the toe position vector results in

$$
\begin{aligned}
px\ =& l_8\left(C_{12}C_3C_{456} + S_{12}S_{456}\right)C_7C_8 \\
& - l_8\left(S_7C_8 + S_{456}S_8\right)C_{12}C_3 + \left(l_7C_{456} - l_9\right)C_{12}C_3C_7 \\
& + \left(l_6 + l_7C_7 - l_9S_7\right)S_{12}S_{456} + l_8S_{12}S_8C_{456} \\
& + \left(l_3 + l_4C_4 + l_5C_{45} - l_7S_7\right)C_{12}C_3 \\
& + \left(l_6 - l_9S_7\right)C_{12}C_3C_{456} + \left(l_4S_4 + l_5S_{45}\right)S_{12} + l_1C_1
\end{aligned} \tag{3}
$$

$$
\begin{aligned}
py\ =& l_8\left(S_{12}C_3C_{456} - S_{456}C_{12}\right)C_7C_8 \\
& - l_8S_{12}\left(S_3S_7C_8 + S_{456}S_8C_3\right) - l_8S_8C_{12}C_{456} \\
& - l_9S_7\left(S_{12}C_3C_{456} + S_{456}C_{12}\right) - \left(l_9C_7 + l_7S_7\right)S_{12}S_3 \\
& + l_7C_7\left(S_{12}C_3C_{456} - S_{456}C_{12}\right) \\
& + \left(l_6C_{456} + l_5C_{45} + l_4C_4 + l_3\right)S_{12}C_3 \\
& - \left(l_4S_4 - l_5S_{45} - l_6S_{456}\right)C_{12} + l_1S_1
\end{aligned} \tag{4}
$$

and

$$
\begin{aligned}
pz\ =& l_8\left(S_3C_{456}C_7 + S_7C_3\right)C_8 - l_8S_3S_{456}S_8 \\
& - l_9S_3S_7C_{456} + l_9C_3C_7 + l_7S_3C_{456}C_7 + l_7S_7C_3 \\
& + \left(l_6C_{456} + l_5C_{45} + l_4C_4 + l_3\right)S_3 - l_2
\end{aligned} \tag{5}
$$

Where $s\theta_i = sin\theta_i$, $c\theta_i = cos\theta_i$, $s\theta_{ij} = sin(\theta_i+\theta_j)$, $c\theta_{ij}=cos(\theta_i+\theta_j)$, $s\theta_{ijk} = sin(\theta_i+\theta_j+\theta_k)$, and $c\theta_{ijk} = cos(\theta_i+\theta_j+\theta_k)$.

Once the forward kinematics is obtained, the next section presents the solution to the inverse kinematics for the legs in Sagittal and Frontal planes.

| DH parameter | Joint | | | | | | | |
|---|---|---|---|---|---|---|---|---|
| | 1 | 2 | 3 | 4 | 5 | 6 | 7 | 8 |
| $\theta_i$ | $\theta_1$ | $\theta_2$ | $\theta_3$ | $\theta_4$ | $\theta_5$ | $\theta_6$ | $\theta_7$ | $\theta_8$ |
| $d_i$ | 0 | $-l_2$ | 0 | 0 | 0 | 0 | $l_7$ | $l_9$ |
| $a_i$ | $l_1$ | 0 | $l_3$ | $l_4$ | $l_5$ | $l_6$ | 0 | $-l_8$ |
| $\alpha_i$ | 0 | $\pi$ | $\pi$ | 0 | 0 | $-\pi$ | $\pi$ | $-\pi$ |

**Table 2.** Right leg DH parameters

## 3. Inverse Kinematics

This section is concerned with finding the solution to the inverse kinematics problem, which consists of determining the joint variables in terms of the end effector position and orientation. It is commonly known in the literature that for open kinematic chains, the determination of closed-form equations for the inverse kinematics represents a greater challenge than the forward kinematics [27].

### *3.1 Inverse Kinematics in the Sagittal Plane*

Figure 2 shows the right leg in the Sagittal plane that describes the motion of the humanoid biped robot, where the base coordinate is at the centre of the toe joint. Note that $\Delta_x$ and $\Delta_y$ are the differential step positions, while $(X_3,Z_3)$, $(X_1,Z_1)$ and $(X_0,Z_0)$ denote the position for the waist, ankle and toe, respectively.

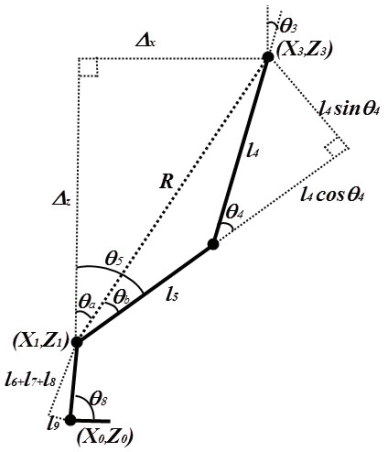


**Figure 2.** Right leg inverse kinematics

The approach that this paper follows for finding the inverse kinematics solution for the right leg in the Sagittal plane consists of determining the joint angle for the knee $\theta_4$, given the global position for the hip and ankle. This work considers that the trajectories of the ankle and hip in the Sagittal plane are known.

Applying the law of cosines to the triangle bounded by $l_4$ and $l_5$ in Figure 2, results in

$$
\cos\left(\theta_4\right) = \frac{R^2 - l_4^2 - l_5^2}{2l_4l_5} \tag{6}
$$

By further using the trigonometric identity atan2, results in the solution for $\theta_4$

$$
\theta_4 = \text{atan2}\left(\sqrt{1 - \left(\frac{R^2 - l_4^2 - l_5^2}{2l_4l_5}\right)^2}, \frac{R^2 - l_4^2 - l_5^2}{2l_4l_5}\right) \tag{7}
$$

where:
$$R^2 = \left(x_3 - x_1\right)^2 + \left(z_3 - z_1\right)^2 \quad (8)$$

The ankle angle $\theta_5$ (see Figure 2) is obtained by adding angles $\theta_a$ and $\theta_b$ as follows

$$\theta_a = \text{atan2}\left(x_3 - x_5, z_3 - z_5\right) \quad (9)$$

$$\theta_b = \text{atan2}\left(l_4 \sin\theta_4, l_5 + l_4 \cos\theta_4\right) \quad (10)$$

and
$$\theta_5 = \theta_a + \theta_b \quad (11)$$

After calculating the ankle and knee angles, the next step is to calculate the hip angle. From geometry it is possible to know that in order to keep the hip of the robot in a vertical position, the ankle, knee and hip angles need to sum zero. Hence, the hip angle $\theta_3$ can be determined as follows

$$\theta_3 = -\theta_4 - \theta_5 \quad (12)$$

Following the same procedure, the toe angle toe $\theta_3$ is

$$\theta_8 = \text{atan2}\left(\frac{\frac{X_3 - X_0 - l_4 sin\theta_4 - l_5 \sin\theta_5}{l}}{\frac{Z_3 - Z_0 - l_4 sin\theta_4 - l_5 \sin\theta_5}{l}}\right) \quad (13)$$

where:
$$l = \sqrt{\left(l_6 + l_7 + l_8\right)^2 + l_9^2} \quad (14)$$

The inverse kinematics for the left leg can be solved with a similar approach as those for the right leg, namely

$$\theta_{11} = -\theta_{12} - \theta_{13} \quad (15)$$

$$\theta_{12} = \text{atan2}\left(\sqrt{1 - \left(\frac{R_1^2 - l_4^2 - l_5^2}{2 l_4 l_5}\right)^2}, \frac{R_1^2 - l_4^2 - l_5^2}{2 l_4 l_5}\right) \quad (16)$$

$$\theta_{13} = \text{atan2}\left(x_{11} - x_{13}, z_{11} - z_{13}\right) + \text{atan2}\left(l_4 \sin\theta_{12}, l_5 + l_4 \cos\theta_{12}\right) \quad (17)$$

and
$$\theta_{16} = \text{atan2}\left(\frac{\frac{X_3 - X_0 - l_4 sin\theta_4 - l_5 \sin\theta_5}{l}}{\frac{Z_3 - Z_0 - l_4 sin\theta_4 - l_5 \sin\theta_5}{l}}\right) \quad (18)$$

Where $\theta_{11}$, $\theta_{12}$, $\theta_{13}$ and $\theta_{16}$ represent the angles of the waist, knee, ankle and toe respectively, in the left leg.

### *3.2 Inverse Kinematics in the Frontal Plane*

Figure 3 shows the model of the motion of the humanoid biped robot in the Frontal plane. Note that the base coordinate is at the centre of the ankle, where $\theta_2$ and $\theta_7$ are the angle in the waist and ankle joint for the right leg, respectively. Likewise, $\theta_{10}$ and $\theta_{15}$ represent the angle in waist and ankle for the left leg, respectively. Additionally, $h$ represents the height of hip joint, and $l_s$ is the width of a step.

Note that $\theta_7$ has been found with trigonometric identities, by using the triangle formed at the articulation of the ankle, hip height and half the width of the step, namely

$$\theta_7 = \frac{\pi}{2} + \text{atan2}\left(y - l_s, h\right) \quad (19)$$

In order to keep the hip of the robot in a vertical position, the ankle, knee and hip angles need to sum $\pi$. Therefore, the hip angle $\theta_2$ can be determined as follows;

$$\theta_2 = \pi - \theta_7 \quad (20)$$

A similar procedure has been used to find the angles $\theta_{15}$ and $\theta_{10}$, for ankle and waist joints in the left leg.

$$\theta_{15} = \frac{\pi}{2} + \text{atan2}\left(y - l_s, h\right) \quad (21)$$

and
$$\theta_{10} = \pi - \theta_{15} \quad (22)$$

Where $y$ represents in Eqs. (19) and (21) the trajectory followed by the hip joint, which is a periodic function and is further introduced in Section 4. Once the forward and inverse kinematics have been determined, the next step consists in proposing all the trajectories that are to be followed by each joint.

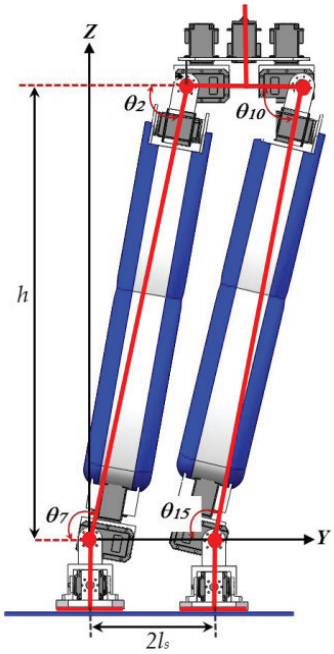


**Figure 3.** Inverse kinematics in Frontal plane

## 4. Trajectory Planning

This work intends to tackle the problem of controlling the biped robot in order to produce walking gait, when the legs follow a desired trajectory. Therefore, it is essential to obtain the desired joint space trajectory given by the Cartesian space trajectory [28]. The points on the following periodic functions are used to determine the rotation angle and thus, calculate the torque of the joints.

$$x_0(t) = \frac{s}{2\pi}\left(\frac{2\pi t}{T_s} - \sin\left(\frac{2\pi t}{T_s}\right)\right) \tag{23}$$

$$z_0(t) = \frac{s_h}{2}\left(\frac{2\pi t}{T_s} - \sin\left(\frac{2\pi t}{T_s}\right)\right) \tag{24}$$

$$x_1(t) = \frac{s}{2\pi}\left(\frac{2\pi t}{T_s} - \sin\left(\frac{2\pi t}{T_s}\right)\right) \tag{25}$$

$$z_1(t) = \frac{s_h}{2}\left(1 - \sin\left(\frac{2\pi t}{T_s}\right)\right) \tag{26}$$

$$x_3(t) = \frac{d}{2\pi}\left(\frac{2\pi t}{T_s} - \sin\left(\frac{2\pi t}{T_s}\right)\right) \tag{27}$$

$$z_3(t) = h \tag{28}$$

and

$$y = s \cdot \sin\left(T_s \pi t\right) \tag{29}$$

Note that Equations (23) to (28) show the periodic functions that describe the biped moving trajectory in the Sagittal plane, while Eq. (29) is the trajectory for the knee in the Frontal plane. Figure 4 shows the trajectory followed by the right leg for one step and the parameters used in the gait trajectory from Eqs. (23) to (28), where $s$ is the length of one step, $s_h$ is the height between the sole of the foot and ground, $d$ is the hip moving distance, $h$ is the height of hip joint, $T_s$ is the period of one step, and $t$ denotes time.

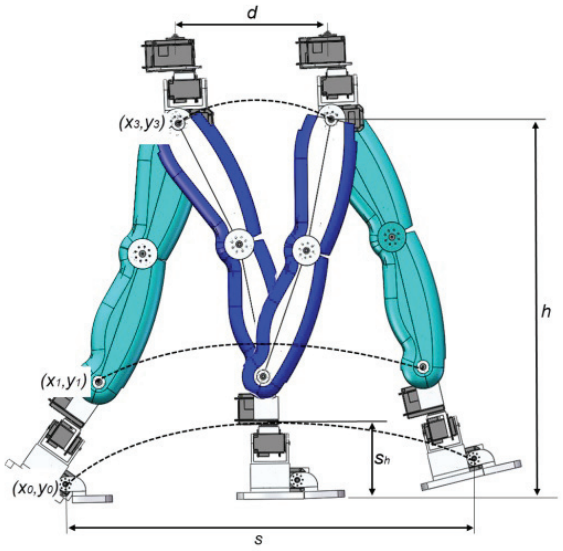


**Figure 4.** Parameters used in trajectory periodic functions

## 5. Dynamics of Humanoid Biped Robot

The approach followed in this paper applies the principles of Lagrangian dynamics for determining the gait locomotion equations for obtaining the torque in each joint of the biped robot. If we recall that in the absence of friction and other disturbances, the Lagrangian $L(q,\dot{q})$ of a mechanical system is defined by

$$L(q,\dot{q}) = K(q,\dot{q}) - P(q) \tag{30}$$

Where $K(q,\dot{q})$ y $P(q)$ represent the kinetic and potential energy of the system, respectively. Note that $q \in \mathbb{R}^n$ represents the vector of generalized coordinates of the system, and $\dot{q} = \frac{d}{dt}q$ is the vector of generalized velocities. The equation of motion of Euler-Lagrange for the humanoid biped robot is given by:

$$\frac{d}{dt}\left(\frac{\partial L(q,\dot{q})}{\partial \dot{q}_i}\right) - \frac{\partial L(q,\dot{q})}{\partial q_i} = \tau_i \qquad i = 1...8 \tag{31}$$

Where $\tau_i \in \mathbb{R}^n$ is the vector of external generalized forces acting on each joint of robot, $q_i$ represents the position of link $i$, and $\dot{q}_i$ is the velocity of link $i$. The kinetic energy for the humanoid robot in the Sagittal plane is calculated by

$$K = \frac{1}{2}\sum_{i=1}^{8}\left(m_i v_i^2 + I_i \dot{q}_i^2\right) \tag{32}$$

Where $I_i$ represents the inertia for link $i$, $m_i$ represents the mass of link $I$ and $v_i$ is the velocity of link $i$. The potential energy for each link can be written as

$$P = \sum_{i=1}^{8} g^T r_{ci} m_i \tag{33}$$

Where $g$ is the gravity vector in the inertial frame and the vector $r_{ci}$ represents the coordinates of the centre of mass of link $i$.

The Euler-Lagrange motion equations provide the following dynamic model [20]:

$$M(q)\ddot{q} + C(q,\dot{q}) + g(q) = \tau \tag{34}$$

Where $M(q) \in \mathbb{R}^{nxn}$ is the inertia matrix, which is symmetric and defined as positive, $C(q,\dot{q}) \in \mathbb{R}^n$ is the vector of centrifugal and Coriolis forces, and $g(q) \in \mathbb{R}^n$ is the vector of gravitational forces.

To calculate the position and torque in each joint, this paper considers a *PD* control law with gravity compensation [29], given by the equation

$$\tau = K_p\tilde{q} + K_v\dot{\tilde{q}} + g(q) \tag{35}$$

Where $K_p, K_v \in \mathbb{R}^{nxn}$ represent the symmetric positive definite matrices, $\tilde{q}$ is the position error and is defined as $\tilde{q} = q_d - q$, where $q_d$ is the desired position, and $\dot{\tilde{q}}$ is the velocity error. The control law in Eq. (35) requires information about the positions $q_d(t)$, $q(t)$ and the velocities $\dot{q}_d(t)$, and $\dot{q}(t)$ at each instant. Figure 5 shows the block diagram corresponding to the *PD* controller with gravity compensation for the humanoid biped robot

The equation that describes the closed loop behaviour is obtained by combining Eqs. (34) and (35) resulting in

$$M(q)\ddot{q} + C(q,\dot{q}) + g(q) = K_p\tilde{q} + K_v\dot{\tilde{q}} + g(q) \tag{36}$$

In this study the motion of the humanoid robot is described in the dynamic model as consisting of two planes, divided by the Sagittal and Frontal planes. This planar model can be compared to a chain of *n* rigid links. In the case of the Sagittal plane, the motion of the humanoid biped robot is modelled by the position *(X, Z)* as shown in Figure 6, where the base coordinate is at the centre of the waist, $(x_0, z_0)$ is the position of point of support, and $(x_f, z_f)$ is the position of the free toe end.

In the case of Frontal plane, the motion is defined by the position *(Y, Z)* as shown in Figure 7, where the base coordinate is at the centre of the waist, $(y_0, z_0)$ is the position of the point of support and $(y_f, z_f)$ is the position of the free toe end. For both planes, the dynamic equations for the humanoid biped robot were presented in [30].

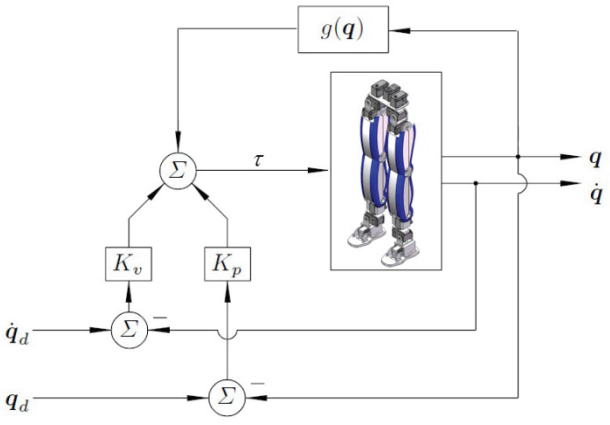


**Figure 5.** *PD* control with gravity compensation for humanoid robot

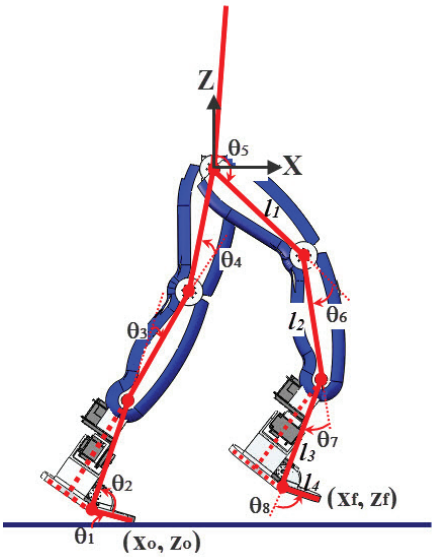


**Figure 6.** Sagittal plane view of the humanoid robot

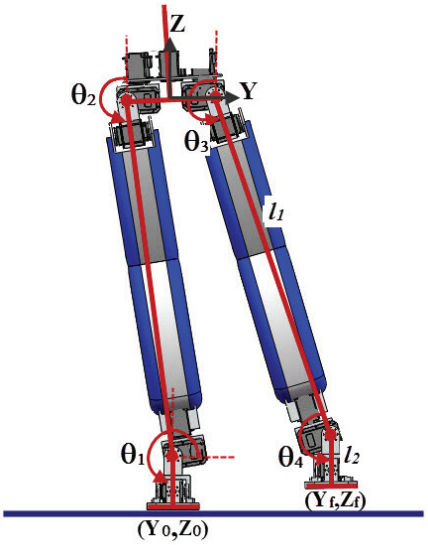


**Figure 7.** Frontal plane view of the humanoid robot

## 6. Numerical Example and Simulation

This work used Maple for producing the numerical examples of the analytical solutions to the kinematics, trajectory planning and dynamics of the humanoid robot. In addition, this paper used SolidWorks and the SimMechanics toolbox from MATLAB for modelling and simulating mechanical systems that use the standard Newtonian laws [31].

### *6.1 Inverse Kinematics and Trajectory Planning*

Table 3 shows the parameters used for the inverse kinematics and trajectory planning in the numerical examples and motion simulations as shown in Fig 2.

| Parameters | Link | Length (m) |
|---|---|---|
| Legs | $l_4 = l_5$ | 0.2 |
| | $l_6 + l_7 + l_8$ | 0.151 |
| | $l_9$ | 0.040 |
| Walking parameters | $s = 0.3\ m$ | |
| | $T_s = 0.25\ Hz$ | |
| | $s_h = 0.05$ | |
| | $h = 0.6\ m$ | |
| | $d = 0.148\ m$ | |

**Table 3.** Dimensional and gait parameters of the humanoid robot

Substituting the parameters from Table 3 into Eqs. (23) to (29), Figure 8 shows the desired gait trajectory for the hip, left, and right foot in dotted, solid and dashed plots respectively, for five steps and with a maximum height of 0.3 m.

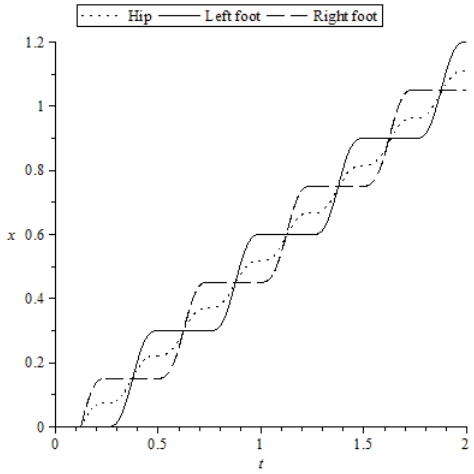


**Figure 8.** Given trajectory for periodic walking

Figure 9 presents the desired feet trajectory for five steps. Note that the maximum height between the sole and the feet is considered to be 0.05 meters.

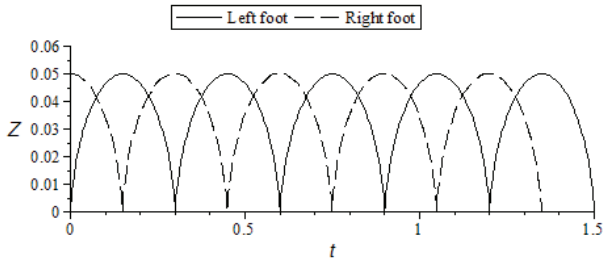


**Figure 9.** Given trajectory for feet in periodic walking

Considering the previously presented gait trajectories in Figures 8 and 9, the position of the right and left legs in the Sagittal plane for joints $q_3$, $q_4$, $q_5$, $q_{11}$, $q_{12}$ and $q_{13}$ is illustrated in Fig. 10 for periodic walking by evaluating Eqs. (6) to (18) for the inverse kinematics in the Sagittal plane. Note that Figure 10 shows the displacement of $q_5$ and $q_{13}$ for the ankle, $q_4$ and $q_{12}$ for the knee, and $q_3$ and $q_{11}$ for the waist for a gait period.

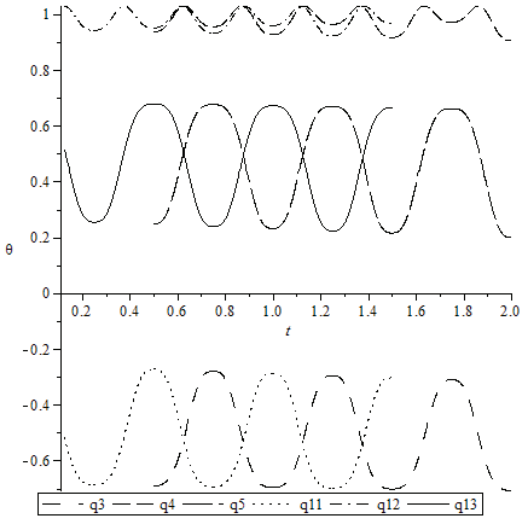


**Figure 10.** Calculated position in Sagittal plane

To verify the analytical results obtained in this paper, SolidWorks and SimMechanics Tool box of MATLAB are used. The model created with the aid of SolidWorks is exported to SimMechanics, where the dynamic simulation is performed. Figure 11 shows the plots for the right and left leg in the Sagittal plane for four steps with a gait period of 0.25. Note that the result given by SimMechanics is similar to the result shown for the numerical example in Figure 10. The simulation parameters (e.g. inertia, mass, and centre of gravity) are imported from the SolidWorks CAD model as shown in Tables 4 and 5.

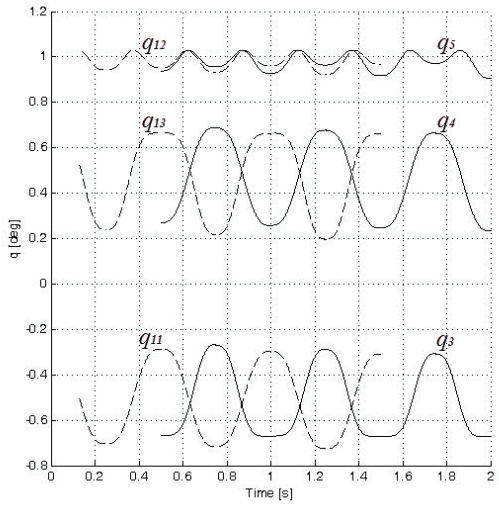


**Figure 11.** Leg position simulation in Sagittal plane

Figure 12 is presented in order to validate the inverse kinematics in the Frontal plane by using Eqs. (19) to (22) to obtain the configuration of the $q_7$ waist joint with a maximum slope of $0.5\pi$. Furthermore, the figure shows the lateral motion in the $q_2$ ankle joint with a maximum slope of $\pi$.

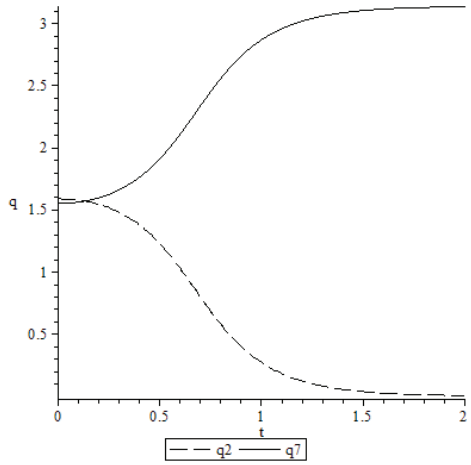


**Figure 12.** Calculated position trajectory for the *q2* joint in waist and *q7* joint in ankle for periodic walking

Following the same approach, Fig. 13 shows the simulation results for the Frontal plane. This simulation represents the lateral motion in the legs for the humanoid; note that the plot is similar to Fig. 12, showing plausibility between the simulation and analytical results.

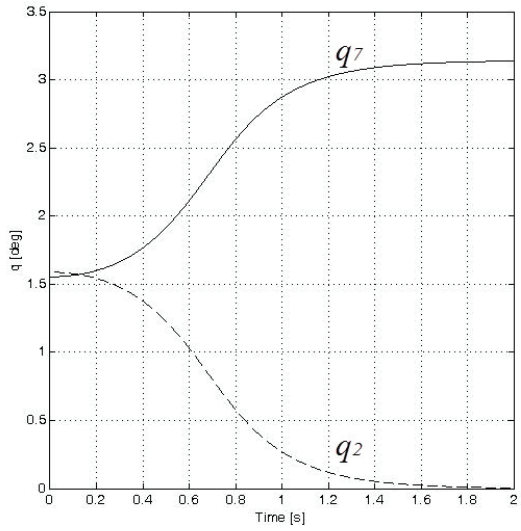


**Figure 13.** Simulation in Frontal plane of legs trajectories

*6.2 Dynamics*

The calculation of the torque for each joint in the Sagittal plane is approached by using Eqs. (30) to (36). Consider a case (i) in which the desired joint positions $q_{di}$ for the link $i$, are chosen as $q_{d1}=\pi/6$, $q_{d2}=0$, $q_{d3}=0$ and $q_{d4}=0$. Table 4 shows the dynamics parameters used in this numeric calculation (see Fig. 6), all values in the Table 4 were obtained from the SolidWorks CAD model. It is possible to see in Figure 14 that the desired position for $q_{d1}=\pi/6$ is achieved at approximate 8 seconds with a torque of 2.8 Nm (see Fig. 15). In addition, Figure 14 shows the position for the other joints $q_{d2}=0$, $q_{d3}=0$ and $q_{d4}=0$, note that the position results are close to zero.

| Link | $m_i\,(kg)$ | $l_i\,(m)$ | $c_i\,(m)$ | $I_i\,(kg\cdot m^2)$ |
|---|---|---|---|---|
| 1 | 1.029 | 0.2 | 0.09864 | 0.00579 |
| 2 | 0.856 | 0.2 | 0.0274 | 0.00398 |
| 3 | 0.757 | 0.158 | 0.0787 | 0.00255 |
| 4 | 0.107 | 0.0786 | 0.00605 | 0.000041 |

**Table 4.** Dynamics parameters of the right leg in Sagittal plane

Figure 15 represents the torque required for $q_1$ in order to achieve the desired position $q_{d1}$ for case (i). The same Figure shows the $T_2$, $T_3$ and $T_4$ torques for the joint $q_2$, $q_3$ and $q_4$. Note that the torque $T_2$ is negative since it is opposite to the motion of $q_1$.

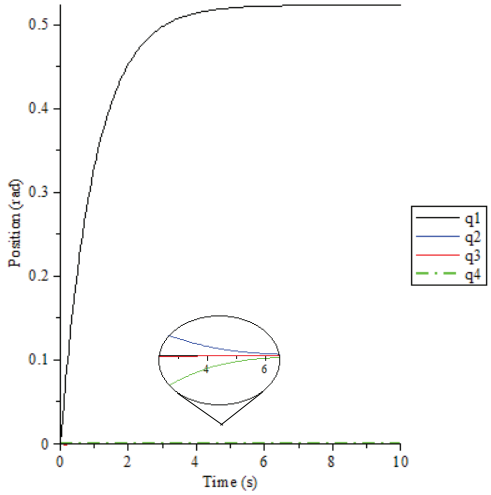


**Figure 14.** Calculated position of joints $q_1$, $q_2$, $q_3$ and $q_4$ for case (i)

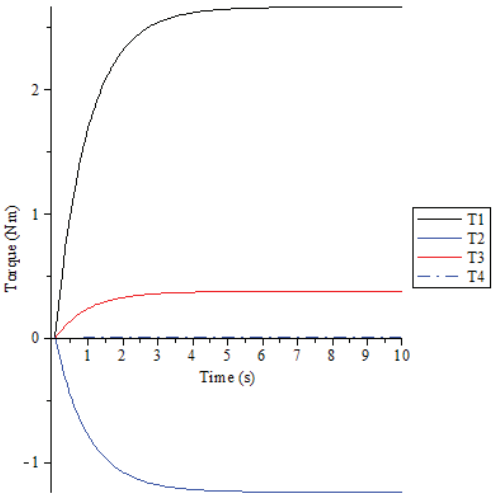


**Figure 15.** Calculated torque of joints $q_1$, $q_2$, $q_3$ and $q_4$ for case (i)

Consider now a case (ii) in Figures 16 and 17 that presents the results for a numeric example when the trajectory is a walking period given by Eqs. (30) to (36), when $q_{d1}=0.0125(8\pi-\sin(8\pi t))/\pi$, $q_{d2}=0$, $q_{d3}=0$ and $q_{d4}=0$. Note in Fig. 16 that the maximum position of the trajectory for $q_1$ when the desired position is $q_{d1}$ = 0.9 rad is reached in 10

seconds with a corresponding torque of 4.153 Nm (see Fig. 17). Furthermore, the Figures show the position and torque for the joint $q_2$, $q_3$ and $q_4$, where it is possible to see that their results are close to zero. Note that the torque $T_2$ is negative because opposes the motion of $q_1$.

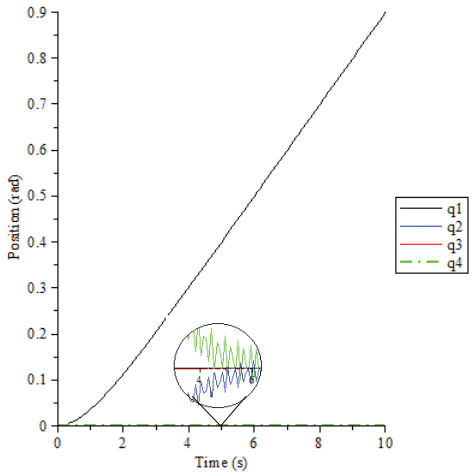


**Figure 16.** Calculated position of joints $q_1$, $q_2$, $q_3$ and $q_4$ for case (ii)

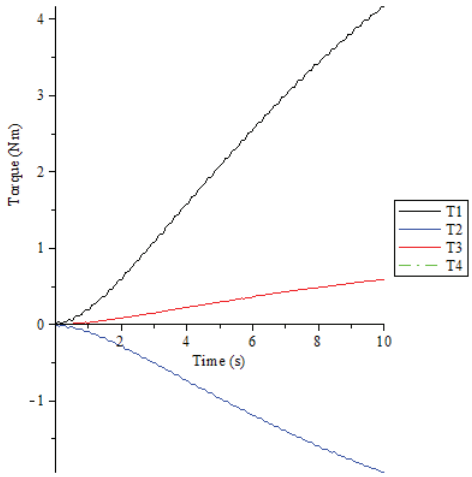


**Figure 17.** Calculated torque of joints $q_1$, $q_2$, $q_2$ and $q_4$ for case (ii)

Similarly to the previous simulation, with the use of Eqs. (30) to (36), it is possible to perform the calculation of the torque for each joint for the Frontal plane. The Table 5 shows the dynamics parameters used in this calculation for the Frontal plane (see Fig. 7), which are obtained from a Solidworks CAD model.

| **Link** | $m_i\,(kg)$ | $l_i\,(m)$ | $c_i\,(m)$ | $I_i\,(kg \cdot m^2)$ |
|---|---|---|---|---|
| 1 | 2.219 | 0.5423 | 0.2438 | 0.05659 |
| 2 | 0.5309 | 0.08235 | 0.0350 | 0.00093 |

**Table 5.** Dynamics parameters of the right leg in the Frontal plane.

Consider now a case (iii) where the desired positions are $q_{d1}=\pi/12$ and $q_{d2}=0$. Note that Figure 18 presents the position for $q_1$ to achieve the desired position $q_{d1}=\pi/12$, which is reached at approximate 3.5 seconds with a torque of 2.3 Nm (see Fig. 19). Furthermore, Fig. 18 and Fig. 19 show the position of joint $q_2$ and torque $T_2$, respectively. Note that the motion of this joint is performed in order to achieve the desired position for joint $q_1$.

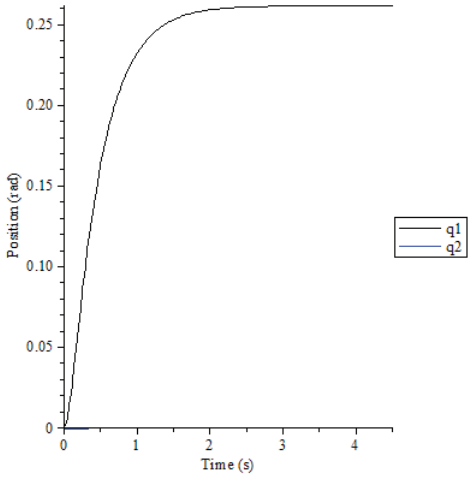


**Figure 18.** Calculated position of joints $q_1$ and $q_2$ for case (iii)

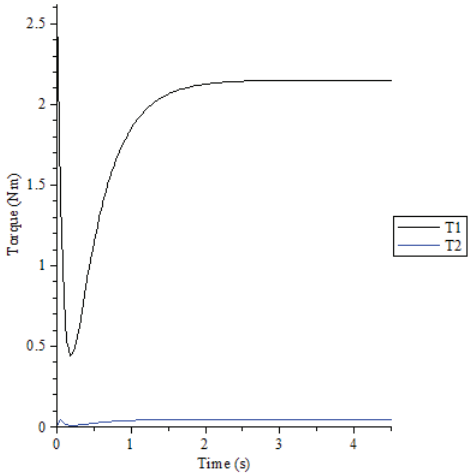


**Figure 19.** Calculated torque of joints $q_1$ and $q_2$ for case (iii)

## 7. Conclusions

This paper presented a new architecture for a biped robot with seven DOF per each leg and an additional DOF that imitates the toe joint.

This work presented the forward kinematics using the DH convention, while the inverse kinematics were approached by decoupling the Frontal and Sagittal planes, resulting in a simplified model that led to closed-form equations for the leg position and orientation.

By considering periodic gait functions, the paper obtained leg trajectories for determining the biped motion and the required torque for each joint. The principle of Lagrangian dynamics applied a PD control law with

gravity compensation in order to control the desired trajectories and to find the torque required by the joints.

Several numerical examples were compared to motion and dynamic simulations, which verified the analytical results.

Future work after this paper will focus on the velocity and acceleration analysis, followed by a singularity analysis in order to identify and eliminate the singular configurations through redundancy. A prototype will be manufactured in order to test alternative algorithms for the gait stability control.

## 8. References


[1] S. Sakagami, R. Watanabe, C. Aoyama, S. Matsunaga, N. Higaki, and F. Fujumura, 2002, "The intelligent ASIMO: system overview and integration", Proc. of the IEEE International Conference on Intelligent Robots and Systems, pp. 2478–2483.

[2] W. Kwon, H. K. Kim, J. K. Park, C. H. Roh, J. Lee, J. Park, W.K. Kim, and K. Roh, "Biped humanoid robot Mahru III", Samsung Electronics Co. Ltd, Suwon-Shi, Kyunggi-Do, pp. 443-742.

[3] Y. Kuroki, T. Ishida, J. Yamaguchi, M. Fujita, and T. Doi, 2001, "A small biped entertainment robot", Proc. of the IEEE/RSJ International Conference on Humanoid Robotics, pp. 181–186.

[4] J. Yamaguchi, E. Soga, S. Inoue, and A. Takanishi, 1999, "Development of a biped humanoid robot control method of whole body cooperative dynamic biped working", Proc. of the IEEE International Conference on Robotics and Automation, pp. 368–374.

[5] N. Nishiwaki, T. Sugihara, S. Kagami, F. Kanehiro, M. Inaba, and H. Inoue, 2000, "Design and development of research platform for perception-action integration in humanoid robot: H6", Proc. of the IEEE International Conference on Intelligent Robots and Systems, pp. 1559–1564.

[6] M. Gienger, K. Loffler, and E. Pfeiffer, 2001, "Towards the design of biped jogging robot", Proc. of the IEEE International Conference on Robotics and Automation, pp. 4140–4145

[7] A. D. Kuo, 2007, "Choosing your steps carefully: Tradeoffs between economy and versatility in dynamic walking bipedal robots" IEEE Robotics and Automation Magazine, Vol. 14, No. 2, June, pp 18-29.

[8] M. Kumagai, and T. Emura., 1997, "Sensor-Based Walking of Humanoid Type Biped Robot ina Curve", Proc. of the JSME Annual Conference on Robotics and Mechatronics, vol. B, pp. 839–840.

[9] K. Kumazawa, and K. Koganezawa., 1998, "Control of Active and Passive Compound Walking", Proc. of the 16th Annual Conference of the Robotics Society in Japan, 3E35, pp. 1121–1122.

[10] Y. Ogura, K. Shimomura, H. Kondo, A. Morishima, T. Okubo, S. Momoki, H. ok Lim, and A. Takanishi., 2006, "Human-like Walking with Knee Stretched, Heel-contact and Toe-off Motion by a Humanoid Robot", Proc. of IEEE International Conference on Robotics and Automation, pp. 3976–3981.

[11] A. Konno, R. Sellaouti, F. B. Amar, and F. B. Ouezdou, 2002, "Design and Development of the Biped Prototype ROBIAN", Proc. of the IEEE International Conference on Robotics & Automation, pp. 1384-1389.

[12] U. Scarfogliero, M. Folgheraiter, and G. Gini, 2004, "Advanced Steps in Biped Robotics: innovative Design and Intuitive Control through Spring-Damper Actuator", Proc. of the International Conference on Humanoid Robots, Humanoids.

[13] K. Koganezawa, and Matsumoto, 2002, "Active/Passive Hybrid Walking by The Biped Robot TOKAI ROBO-HABILIS 1", Proc. of the IEEEIRSJ Intl. Conf. on Intelligent Robots & Systems, pp. 2461-2466.

[14] K. Nishiwaki, S. Kagami, Y. Kuniyoshi, M. Inaba, and H. Inoue, 2002, "Toe Joints that Enhance Bipedal and Fullbody Motion of Humanoid Robots", Proc. of the IEEE International Conference on Robotics and Automation, pp. 3105–3110.

[15] R. Sellaouti, O. Stasse, S. Kajita, K. Yokoi, and A. Kheddar, 2006, "Faster and Smoother Walking of Humanoid HRP-2 with Passive Toe Joints", Proc. of the 2006 IEEE/RSJ International Conference on Intelligent Robots and Systems, October 9 - 15, Beijing, China.

[16] R. Prasanth Kumar, Jungwon Yoon, Christiand, and Gabsoon Kim, 2009, "The simplest passive dynamic walking model with toed feet: a parametric study", Robotica, volume 27, pp. 701–713, Cambridge University Press.

[17] M. Vukobratovic, V. Potkonjak, and S. Tzafestas, 2004, "Human and Humanoid Dynamics", Journal of Intelligent and Robotic Systems, Vol. 41, pp 65–84, the Netherlands.

[18] A. Kun, and W.T. Miller, 1996, "Adaptive dynamic balance of a biped robot using neural networks", Proc. of the IEEE International Conference on Robotics and Automation, pp. 240–245.

[19] M. Vukobratović, V. Potkonjak, K. Babković, and B. Borovac, 2007, "Simulation model of general human and humanoid motion", Multibody System Dynamics, Vol. 17, No. 1, pp. 71-96.

[20] V. S. Cvetkovic, 1977, "Postural stability of two biped models via Lyapunov second method", IEEE Trans. Automatomatic Control, vol. AC-22, pp. 64-70.

[21] P.R. Vundavilli, and D. K. Pratihar, 2011, "Balanced gait generations of a two-legged robot on sloping surface", Indian Academy of Sciences Sadhana , Vol. 36, Part 4, August 2011, pp. 525–550.

[22] L. C. Kwek, E. K. Wong, C. K. Loo, and M. V. C. Rao, 2003, "Application of Active Force Control and Iterative Learning in a 5-Link Biped Robot", Journal of Intelligent and Robotic Systems, Vol. 37, pp. 143–162.

[23] Rodriguez Leal, E., Dai, J.S., and Pennock, G.R., 2011, "Kinematic Analysis of a 5-RSP Parallel Mechanism with Centralized Motion", Special Issue: Fundamental issues and new trends of parallel mechanisms and manipulators, Meccanica, Springer Verlag, 46(1), pp. 221-237.

[24] S.G. Tzafestas, and T.E. Krikochoritis, 1997, "Robust Sliding-mode Control of Nine-link Biped Robot Walking", Journal of Intelligent and Robotic Systems, Vol. 20, pp. 375–402.

[25] C. Hernández-Santos, R. Soto, and E. Rodríguez, 2011, "Design and Dynamic Modeling of Humanoid Biped Robot e-Robot", Proc. of the IEEE Electronics, Robotics and Automotive Mechanics Conference, CERMA 2011, pp. 191-196, Cuernavaca, México.

[26] C. Chevallereau, G. Bessonnet, G. Abba, Y. Aoustin, 2009, "Bipedal Robots, Modeling, Design and Walking Synthesis", Ed. Wiley

[27] A. Faller, M. Schünke, and G. Schünke, 2004, "The Human Body: An Introduction to Structure and Function", Ed. Georg Thieme Verlag.

[28] J. Denavit, and R. S. Hartenberg, 1955, "A kinematic notation for lower pair mechanisms based on matrices," Trans ASME Journal of Applied Mechanisms, Vol. 23, pp. 215–22.

[29] K. S. Fu, R. C. Gonzalez, and C. S. G. Lee, 1987, "Robotics: Control, Sensing, Vision, and Intelligence", McGraw-Hill.

[30] T.T. Lee, and J.-H. Liao, 1988, "Trajectory planning and control of a 3-link biped robot", Proc. of the 1988 IEEE International Conference on Robotics and Automation, Vol. 2, pp. 820-823.

[31] C. Hernández-Santos, E. Rodriguez-Leal, R. Soto, and J.L. Gordillo, 2012, "Kinematics and dynamics of a new 16-DOF humanoid biped robot", Proc. of the ASME 2012 International Design Engineering Technical Conferences, accepted for publication.